



# Integrated approach in studying rock and soil slope stability in a tropical and active tectonic country

Ibnu Rusydy<sup>1,5</sup> · Teuku Faisal Fathani<sup>2</sup> · Nafisah Al-Huda<sup>1,3</sup> · Sugiarto<sup>3</sup> · Khairul Iqbal<sup>3</sup> · Khaizal Jamaluddin<sup>3,4</sup> · Ella Meilianda<sup>3,5</sup>

Received: 21 September 2019 / Accepted: 23 December 2020 / Published online: 11 January 2021  
© The Author(s), under exclusive licence to Springer-Verlag GmbH, DE part of Springer Nature 2021

## Abstract

An integrated study on slope stability has been conducted in the high weathering zone of the tropical and active tectonic country, Indonesia. The research aims to introduce an integrated and comprehensive approach in studying the soil and rock slope stability. Geophysical methods, including two seismic refraction tomography (SRT) and electrical resistivity tomography (ERT) lines, were deployed to determine the slip zone of the landslide. Slope kinematic analysis and rock mass classification were performed on the slope surface for obtaining data of engineering geology combined with Standard Penetration Test (SPT) data collected next to the sloping road. The soil slope stability analysis was simulated by employing the Slope/W software to determine the factor of safety. The geophysical methods revealed three layers of rock and soil on top of the rock layer, showing the slip zone of the landslide. The kinematic analysis revealed the planar failure, which possibly occurred in Site B of Babarot—Gayo Lues road in Aceh Province due to the parallelism between slope and joint. The integrated data from the geophysical methods and in situ RMR indicate that the rock mass classification in sub-surface is classified as Very Good and Good Rock. It appears to be stable. The soil above the slope in sites A and B has 1.058 and 1.182 factor of safety, respectively; yet, it has less than 0.847, the factor of safety, when loaded by the earthquake and it is unstable.

**Keywords** Slope stability · Rock mass classification · Geophysical methods · Geotechnical

## Introduction

Indonesia exemplifies typical Southeast Asian countries influenced by the monsoonal climate (Wang et al. 2009), where seasonal variations of dry and rainy months occur

annually. The Indonesian archipelago is one of the most tectonically-active regions on the planet earth, located near the subduction zones of the colliding Indo-Australia and Euro-Asian (Eurasia) tectonic plates. On the north tip of Sumatra Island of Indonesia, Aceh Province experiences a high frequency of earthquake occurrences, combined with rainy seasons, typically from September to February. Despite the inherent influence of temperature, such a combination promotes chemical weathering induced by heavy rainfall (Liu et al. 2012). The weathering may be responsible for the rock to lose its strength, which affects all of the engineering properties of rocks and will reduce the shear strength and stability of rocky slopes (Jayawardena and Izawa 1994; Xue et al. 2018; He et al. 2011). Furthermore, in the southern part of Aceh, a subduction zone is present between the Indo-Australia plates and the Eurasia plate where the Indo-Australia plate moves northward and is subducted beneath the Eurasia plate at approximately 5 cm/year (McCaffrey 2009) and the Great Sumatra Fault (GSF) zone is located near the study area; hence, both subduction zone and GSF are possible to

✉ Ibnu Rusydy  
ibnu@unsyiah.ac.id

<sup>1</sup> Department of Geological Engineering, Faculty of Engineering, Universitas Syiah Kuala, Banda Aceh, Indonesia

<sup>2</sup> Center for Disaster Mitigation and Technological Innovation (GAMA-InaTEK, Universitas Gadjah Mada, Yogyakarta, Indonesia

<sup>3</sup> Department of Civil Engineering, Faculty of Engineering, Universitas Syiah Kuala, Banda Aceh, Indonesia

<sup>4</sup> Department of Geophysical Engineering, Faculty of Engineering, Universitas Syiah Kuala, Banda Aceh, Indonesia

<sup>5</sup> Tsunami and Disaster Mitigation Research Center (TDMRC), Universitas Syiah Kuala, Banda Aceh, Indonesia

produce a high magnitude of the earthquake interfering the stability of the slope.

Slope stability studies are crucial for slope failure mitigation, for instance, along the roadside, thus, reducing the loss of life, property damage, and environmental degradation. The roadside slope failures could disrupt the transportation network and affect the logistics mobilization between two distant places. At Babahrot and Gayo Lues districts in Aceh Province, numerous slope failures have occurred in recent years. Along the road, in particular, the weathering layer (soil) is sitting on top of the rock layers causing instability of the slopes, consequently disrupting the transportation network and affect the logistics mobilization. To propose a sound mitigation strategy for the foreseeable slope failure, an integrated analysis of geophysics, geotechnical, engineering geology methods is, therefore needed.

Previously, various studies on slope stability have been conducted by applying geophysical, geotechnical, and engineering geology approaches. Regarding the geophysical method, the research on slope stability has been introduced by Bogoslovsky and Ogilvy (1997), Hack (2000), Glade et al. (2005), and Jongmans and Garambois (2007). They successfully employed the seismic refraction tomography (SRT) in determining the depth of landslide slip surface. Furthermore, Bogoslovsky and Ogilvy (1997), Lebourg et al. (2010), and Di Maio et al. (2020) identified the thickness of the landslide body and soil saturation degree by deploying the electrical resistivity tomography (ERT) method while Syukri et al (2020) utilised the ERT to determine the cause of road pavement failure. Nevertheless, they did not develop a limit equilibrium analysis to produce a factor of safety (FoS) and only considered a landslide slip surface. As for the geotechnical approach, Avanzi et al. (2013) introduced the Standard Penetration Test (SPT) measurement and soil properties analyses for shallow landslide, while the slope stability simulation using limit equilibrium analysis have been conducted by Das and Sobhan (2013), Abdalla et al. (2015) and Kassou et al. (2020). Gunawan et al. (2020) and Isa et al. (2018) conducted slope stability simulation which considers the effect of rainwater to slope, while the influence of rainwater infiltration. All those research performed the SPT combined with soil sampling to determine the heterogeneous geo-materials on the slope but have yet to consider the quality of rock mass beneath the soil layers.

Furthermore, rock mass classification as one of the engineering geology methods is the backbone of rock mass quality analysis and an empirical design approach for rock slope stability (Rusydy et al. 2017, 2019, 2020c). The application of surface rock mass classifications for slope stability analysis has been conducted by Basahel and Mitri (2017), Wei et al. (2020), and Rusydy et al. (2017, 2019, 2020c), without further consideration of rock mass classification in sub-surface, which influences the stability of the slope.

Furthermore, multidisciplinary approach considering the morphologic, geological setting, geo-structural data of rock slope, groundwater, and its impact to human has been conducted by Andriani and Liotine (2020). All previous studies in soil and rock slope stability are considered as stand-alone studies, and there are gaps among those approaches. This study tries to fill the gap using an integrated and comprehensive analysis of soil stability and rock slope; therefore, it will produce reliable results. Therefore, the purpose of this research is to discuss an integrated approach in soil and rock slope stability study in a tropical country that is prone to tectonic activities. Furthermore, this study will provide a comprehensive method in field data acquisition by combining geophysical method along with geotechnical and engineering geology methods.

In general, this study discusses the rock mass classification systems from an engineering geology perspective, its correlation with geophysical data and geotechnical data, and its implementation in slope stability studies after being disturbed by the earthquake's dynamic load static stages of groundwater. The final result is the factor of safety of the slope at different stages of groundwater and earthquake dynamic load. These processes will yield reliable results in slope stability analysis for tropical and active tectonic country.

## Tectonic setting and geology of study area

The Babahrot–Gayo Lues Road is located 332 km southeast of Banda Aceh City, Indonesia (see Fig. 1). Numerous landslides have occurred; as a result, it disconnected Babahrot and Gayo Lues District of Aceh province, Indonesia. The numbers of rock units observed along the Babahrot–Gayo Lues road denoting the geological processes in the past. According to Cameron et al. (1982), various extrusive igneous rock units of different ages were found in this area, and they formed from the late Jurassic (163.5 million years ago) to the early Cretaceous (100.5 million years ago). Barber and Crow (2005) defined these units of rocks as the oceanic assemblage, especially the basaltic-andesitic arc assemblage, which is part of the Babahrot Formation in the Woyla Group. Unweathering (fresh) rock is difficult to find in this study area due to the rapid weathering processes in tropical countries.

After the Babahrot Formation (Mult) was deposited, another igneous rock was formed in the late Oligocene to early Miocene. This rock was named Sapi Volcano Formation (Tlvs), which consists of andesitic lava rock. This andesite unit can be observed from 9 km to 13.4 km along Babahrot–Gayo Lues road. During the same epoch, sedimentary rock consisting of shale and sandstone was formed in this area, part of the Leuser Formation (Tll).

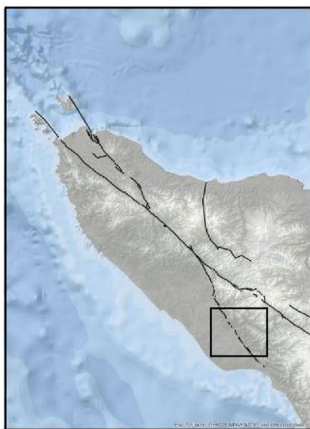
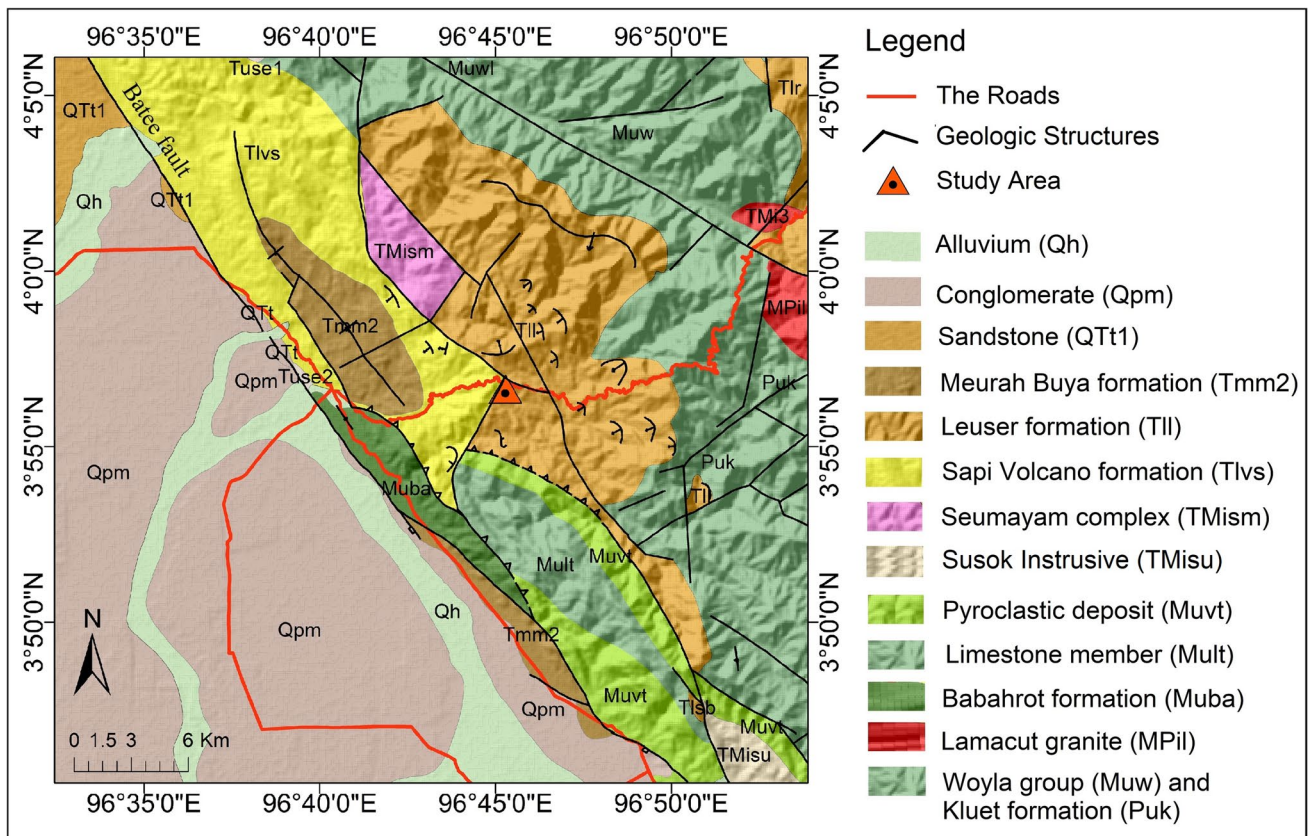


**Fig. 1** Indonesia archipelago derived from Google Map, Sumatra fault lines in Aceh province and the geology map of study area modified from Cameron et al. (1982)

Shale in the Leuser Formation is formed from alluvial processes, and it can be found from 14 km until the Gayo Lues district, and it is exactly located in the investigated slope. The sandstone can be observed for 24.4 km along this road. The shale and sandstone do not lay in the horizontal layer. As a result, the bedding trace dip in this study area is relative to the south (Cameron et al. 1982). The highly weathered shale is found on the surface of the slope in

the study area. We observed the residual and depositional soil forming on top of shale bedding, and this residual soil becomes the source of the landslide.

Several rockfalls occurred due to the high discontinuous features of the rock caused by tectonic forces from the subduction zone between the Indo-Australia and Eurasia plates and the Great Sumatra Fault (GSF) zone. The GSF is an active fault system that possibly generates earthquakes in

the future (Muksin et al. 2018; Rusydy et al. 2018, 2020a). The dynamic load of the earthquake can put the slope in an unstable stage. As shown on the map (see Fig. 1), the Batee fault segment, which is part of GSF, is situated 7 km to the south-west of the study area, facilitating the studied area prone to earthquakes. Besides, as an active tectonic country, the rock in this study area is highly fractured by tectonic force and weathering process. Hence, an integrated study, especially on topsoil and rock quality as well as stability beneath the soil, becomes compulsory in Indonesia.

## Methodology

As the integrated research, numerous stages have been taken in data acquisition, data analysis and processing, interpretation, and following by rock and soil slope stability simulation. More detail each approach taken in this study can be seen in this section and the research flowchart as denoted in Fig. 2.

## Geophysical investigation

The combination of geophysical methods and geotechnical testing to investigate landslides has been utilized by Glade et al. (2005) and Friedel et al. (2006). The geophysical approach works based on physical properties of earth materials (Telford et al. 1990). This study combines 2D

seismic refraction tomography (SRT) with 2D electrical resistivity tomography (ERT) data to investigate the thickness of the landslide body and the slip zone at site A and geo-material properties beneath the surface (see Fig. 3).

SRT deploys seismic wave propagations in sub-surface refracted to the surface. The key assumption in SRT for investigating landslide slip zones is the difference in elasticity and stiffness on the slip zone layer to the layers above. Accordingly, this stiffness contrast yields a different value in P-wave velocity  $V_{PF}$  (Glade et al. 2005; Zikrilah et al. 2016). A 4 kg sledgehammer was used as a seismic source recorded by 24 geophones and 5 blows were consecutively stacked to avoid the noise from plant root vibrations and other noise sources. Twenty four sets of 10 Hz geophones were installed 2 m apart as suggested in Zikrillah et al. (2016). Two seismic lines were acquired over the sloped terrain and road using PASI seismometer equipment (see Fig. 3). Subsequently, data processing and analysis were carried out using the ZondST2D software developed by Kaminsky (2015). The ZondST2D software picks every seismic signal by its first-time arrival, and assumes the SRT velocity ( $V_{PF}$ ) is proportionally escalating with depth. The SRT velocity ( $V_{PF}$ ) has high correlation to the quality of rock mass. Accordingly, it can be used to estimate the RMR, GSI and SMR value in the sub-surface. The ZondST2D software works based on refraction waves forward modelling and inversion in arbitrary layered medium (Kaminsky 2015).

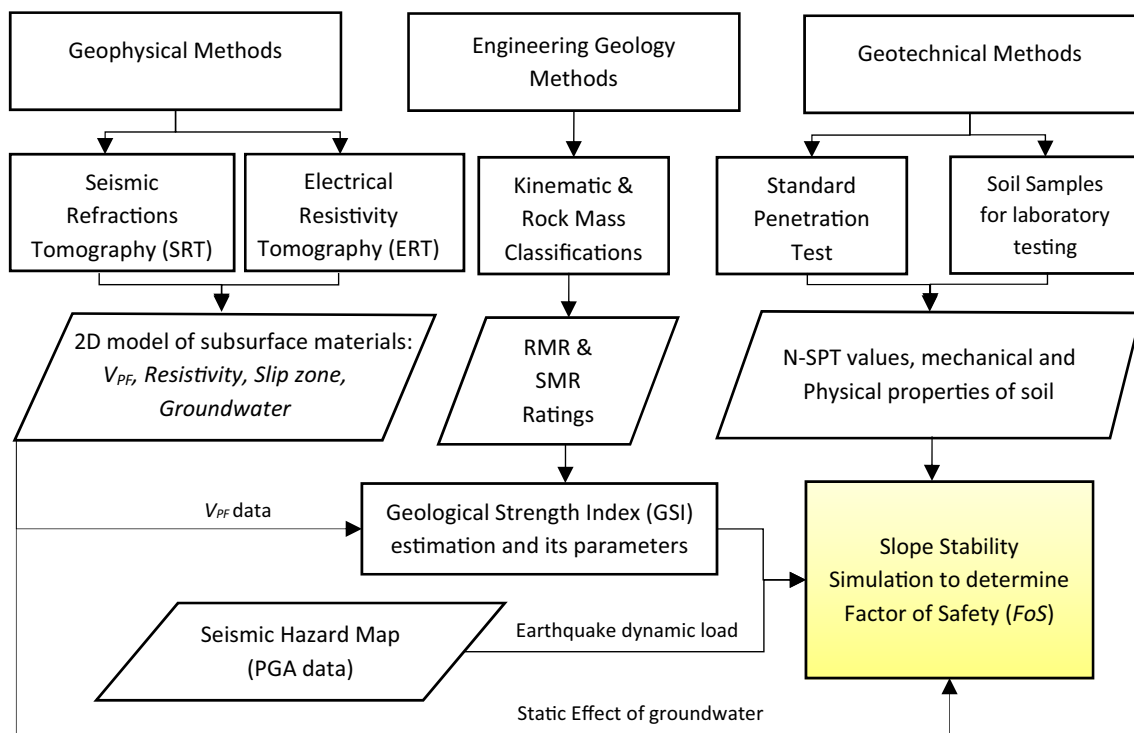


**Fig. 2** Flow chart of integrated approach in analysing rock and soil slope stability in tropical and active tectonic country

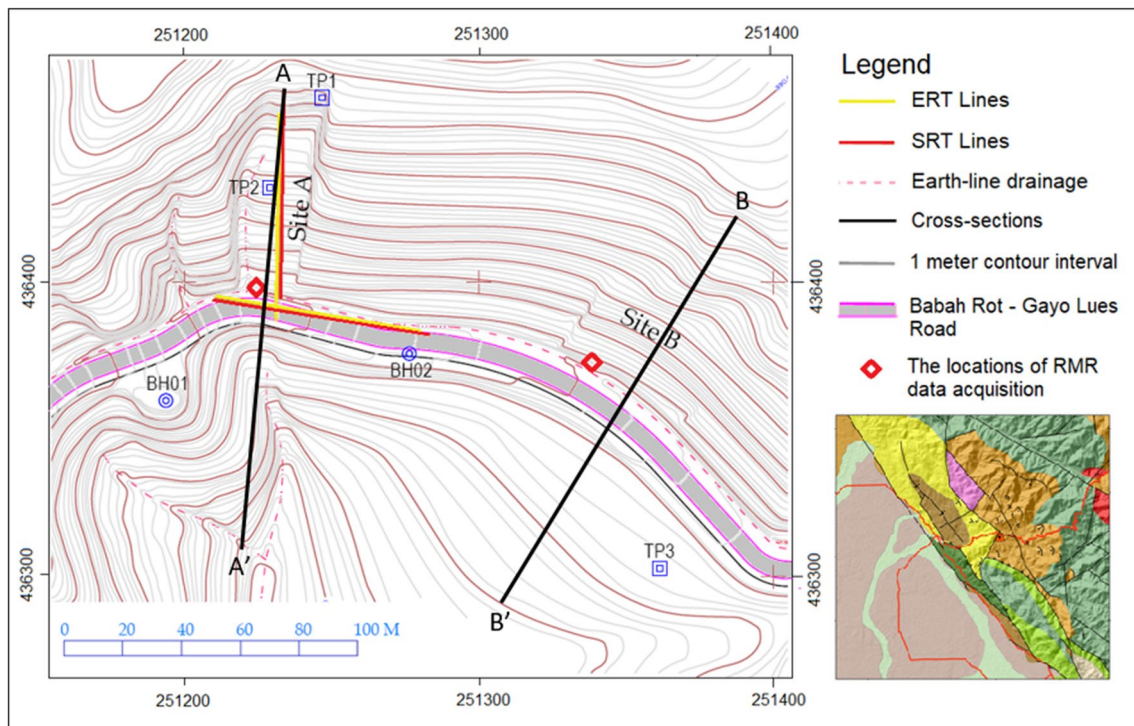


**Fig. 3** The location of SRT and ERT lines profile on the slope and beside the road, the N-SPT and, Test Pit location. BH01, BH02 is the location N-SPT and TP1, TP2, and TP3 for Test pit location. The topography map of study area in UTM 47 N coordinate system

The second geophysical method employed is ERT method in determining the sub-surface layer based on electrical characteristics, including the resistivity and chargeability of soil or rock (Telford et al. 1990; Sugiyanto et al. 2018; Rusydy et al. 2020b). The ERT method performs by penetrating an electrical current along numerous paths through the sub-surface and determine geo-material characteristics based on the resistivity property of the earth materials (Telford et al. 1990; Rusydy et al. 2020b); this technique has been well established since the 1990s (Lebourg et al. 2010).

The 2D ERT technique was employed to investigate the landslide slip zone because soft-sediment above slip zone has high porosity; consequently, it will yield high resistivity located above in the slip zone (Friedel et al. 2006). In addition, the ERT method is capable of recognizing the groundwater level, water content, moisture contents, and degree of saturation in the sub-surface (Fukue et al. 1999; Uhlemann et al. 2017; Di Maio et al. 2020). Furthermore, Lebourg et al. (2010) acknowledge that the resistivity value strongly correlates with the rise of the piezometric level on the slope. When the geo-materials are saturated with groundwater, the electrical conductivity of those materials will increase, while the resistivity is decrease. In this study, two ERT lines profiles, as shown in Fig. 3, lie on the slope and the road and a SuperSting R8/IP resistivity meter with a length of 82.5 m were used for data acquisition. The SuperSting R8/IP is a

multi-electrode system resistivity meter that consists of conventional steel electrodes. The Schlumberger-configuration electrodes were applied; the spacing between each electrode was 1.5 m to provide sufficient resolution for slip zone determination on the slope and groundwater. The data analysis was conducted by employing 2D Earth Imager software. Also, the elevation data along each profile were measured using a Cobra 4 Phywe altimeter for the SRT and ERT lines.

### Geotechnical investigation and soil stability analysis

A Standard Penetration Test (SPT) and soil laboratory testing were conducted for the geotechnical investigation in two locations next to the road at BH01 and BH02. In addition, three test pits, TP1, TP2, and TP3, were conducted on the slope (see Fig. 3) to collect numerous samples of the soils which were then analysed in the laboratory. SPT is a standard method for a civil engineer to investigate the sub-surface soil quality. According to ASTM D1586-11 (2011), the test process works on the lower part of the borehole where a split-barrel sampler which has an inner diameter of either 38.1 mm or 34.9 mm is driven into the sub-surface using a hammer for a given distance of 0.30 m after a seating interval. The hammer weighs approximately 623-N and it falls from  $0.76 \pm 0.030$  m in each hammer blow; the N-value

(N-SPT value) was recorded as the number of hammer blows per foot of penetration representing the resistance of the soil.

The soil properties from the SPT sampling and test pit samplings were analysed in the laboratory. The depth of soil in our study area is shallow soil, and the type of landslide is a shallow landslide. SPT and soil properties analyses for shallow landslide was introduced by Avanzi et al. (2013). The two soil investigation areas are appropriate for our study area where the soil sampling and analysis will yield the soil classification result based on the AASHTO (America Association of State Highway and Transportation Officials) and the USCS (The Unified Soil Classification System). These classifications were performed because the boundary or transition between the soil and rock zones was not well defined, and the RMR system in very weak rock to soil is difficult to perform for practical reasons (Warren et al. 2016).

Slope stability simulation was developed based on the concept of boundary balance; it assumes that the failure occurs along a specified landslide area, while the value of the shear strength along the potential landslide plane is calculated and compared with the shear resistance along the potential failure surface. This comparison is defined as a factor of safety (FoS) for the slope (Abramson et al. 2001; Das and Sobhan 2013; Abdalla et al. 2015) and accordingly, this study employed the Slope/W software in the analysis of the factor of safety of the slope in consideration of dynamic load of the earthquake.

Hoek–Brown failure criterion introduced by Hoek et al. (2002) was utilized to analyse the rock slope stability beneath the soil and Mohr–Coulomb for the soil in limit equilibrium analysis. The Hoek–Brown failure criterion has a high relationship to geological data and its failure equation is expressed as follows:

$$\sigma'_1 = \sigma'_3 + \sigma_{ci} \left( m_b \frac{\sigma'_3}{\sigma_{ci}} + S \right)^a \quad (1)$$

$$m_b = m_i \exp \left( \frac{GSI - 100}{28 - 14D} \right) \quad (2)$$

where the  $\sigma_1$  and  $\sigma_3$  are the major and minor effective principal stresses at failure, while  $\sigma_{ci}$  is the uniaxial compressive strength (UCS) of the intact rock material that can be estimated from the field. The  $S$  and  $a$  are constant from the rock and calculated using the following equation:

$$S = \exp \left( \frac{GSI - 100}{9 - 3D} \right) \quad (3)$$

$$a = \frac{1}{2} + \frac{1}{6} (e^{-GSI/15} - e^{-20/3}) \quad (4)$$

The value of  $D$  (disturbance factor) and the  $m_i$  depends on the type of rock, those parameters refer to Hoek et al. (2002).

In addition, the value of GSI was derived from the rock mass classification analysis and will be used as the input data to the Slope/W software for the slope simulation.

## Rock mass classification analysis

The rock mass classifications were introduced by Ritter in 1879 when he attempted to formulate an empirical approach for tunnel design and the support system (Rai et al. 2014; Mohammadi and Hossaini 2017). The rock mass classifications were also employed in this study. Many rock mass classifications employ multiple parameters developed from civil engineering case studies. Rock mass classifications include RMR (Rock Mass Rating) from Bieniawski (1989), SMR (Slope Mass Rating) by Romana (1985), Q-System by Barton et al. (1974), GSI by Hoek and Brown (1997), and many others developed to determine the rock mass quality for tunnel and slope design.

According to Singh and Goel (1999), rock mass classification provides basic empirical design and is widely used in rock engineering, called the quantitative rock mass classification system. This system bridges and provides better communication between geologist, designers, contractors and civil engineers; the most widely known and used rock mass classifications are the RMR system of Bieniawski (1989), the Q-system of Barton et al. (1974), and the GSI proposed by Hoek and Brown (1997). For evaluation of slope stability, Romana (1985) developed a new adjustment factor to the RMR system of Bieniawski (1989) called the Slope Mass Rating (SMR). The application of the rock mass classification systems in slope stability analysis was introduced by Basahel and Mitri (2017), Wei et al. (2020), Rusydy et al. (2017, 2019, 2020c).

## Rock slope kinematic analysis

This study performs a slope kinematic analysis to determine the slope stability based on the type of rock mass movement without any consideration of the cause of movement (Gurocak et al. 2008; Rusydy et al. 2017, 2019, 2020c). In this method, the structural geology knowing as discontinuity data are determined for the slope including bedding, joints, folds, fractures, and faults; these structures have a strong effect on the rock slope stability (Wyllie and Mah 2004; Grelle et al. 2011; Siddique and Khan 2019; Rusydy et al. 2016, 2017, 2019, 2020c). Engineering geologists commonly employ kinematic analyses and rock mass classifications for slope and tunnel design.

## Rock mass rating (RMR)

RMR was developed at the South African Council of Scientific and Industrial Research (CSIR) initiated by Bieniawski in

1973; Since then, the RMR has undergone several significant changes and the latest one is RMR system of Bieniawski in 1989 (Singh and Goel 1999). RMR was initially developed on case histories from civil engineering projects. Hence, the most recent RMR in 1989 included modifications for mining purposes (Hoek 2007).

The RMR parameters presented in Table 1 classifies the geologic structure into various ratings to calculate the total RMR value, which range value is given to prevent from subjective interpretations. In addition, Nourani et al. (2017) proposed an equation for estimating the RMR from the P-wave velocities in the field ( $V_{PF}$ ), as mentioned in Eq. 5, where the velocity unit is in km/s. The uniaxial compressive strength (UCS) can be derived from field estimation using a geologic hammer and pocket knife as described by Hoek (2007), while the RQD was computed by deploying new correlations between the volumetric joint ( $J_v$ ) and RQD equations, as proposed by Palmstrom (2005). It is shown in Eq. 6. The  $J_v$  value is equal to one spacing of discontinuity planes.

$$RMR = 54.541 + 8.272 V_{PF} \tag{5}$$

$$RQD = 110 - 2.5 J_v \tag{6}$$

In this study, the estimation of the RMR value beneath the surface is calculated using Eq. 5 based on the SRT value ( $V_{PF}$ ). In addition, this study calculated the Geological Strength Index (GSI) from the RMR value by utilizing Eq. 7; GSI is the recent rock mass classification proposed by Hoek and Brown (1997).

$$GSI = RMR - 5 \text{ for } RMR \geq 23 \tag{7}$$

**Slope mass rating (SMR)**

The SMR was proposed by Romana (1985) as an additional adjustment to Bieniawski’s RMR system for slope analysis considering the relationship between the strike and dip of the slope and the strike and dip of joints on the slope. The equations proposed by Romana (1985) are shown in Eq. 8, 9 and, 10.

$$SMR = RMR + (F_1 \cdot F_2 \cdot F_3) + F_4 \tag{8}$$

**Table 1** The parameters of Rock Mass Rating system after Bieniawski (1989)

Parameters		Range of values							
1	Strength of intact rock material	Point load strength index	> 10 MPa	4–10 MPa	2–4 MPa	1–2 MPa	For this low range, UCS test is preferred		
		Uniaxial compressive strength (ucs)	> 250 MPa	100–250 MPa	50–100 MPa	25–50 MPa	5–25 MPa	1–5 MPa	< 1 MPa
	Rating		15	12	7	4	2	1	0
2	Rock quality designation (rqd)		90–100%	75–90%	50–75%	25–50%	< 25%		
		Rating	20	17	13	8	3		
3	Spacing of discontinuities		> 2 m	0.6–2 m	200–600 mm	60–200 mm	< 60 mm		
		Rating	20	15	10	8	0		
4	Condition of discontinuities		Very rough surfaces, not continuous	Slightly rough surfaces	Slightly rough surfaces	Slickensided surfaces or gouge < 5 mm thick or separation 1–5 mm	Soft gouge > 5 mm thick or separation > 5 mm		
			No separation	Separation < 1 mm	Separation < 1 mm	Highly weathered walls	Continuous		
			Unweathered wall rock	Slightly weathered walls					
	Rating		30	25	20	10	0		
5	Ground water	Inflow per 10 m tunnel length (l/m)	0	< 10	10–25	25–125	> 125		
		(Joint water-pressure)/(major principal, $\sigma$ )	0	< 0.1	0.1–0.2	0.2–0.5	> 0.5		
		General conditions	Completely dry	Damp	Wet	Dripping	Flowing		
	Rating		15	10	7	4	0		

$$F_1 = [1 - \sin(\alpha_s - \alpha_j)]^2 \tag{9}$$

$$F_2 = \tan\beta_j \tag{10}$$

where  $F_1$ ,  $F_2$ ,  $F_3$ , and  $F_4$  are the adjustment factors related to the relationship between slope orientation and joints orientation.  $\alpha_s$  is the slope strike,  $\alpha_j$  is the joint strike, and  $\beta_j$  are the joint dips. The  $F_1$  value is calculated using Eq. 9, and it describes the parallelism between the joint strike and slope strike.  $F_2$  is computed using Eq. 10, and it refers to the relationship between the slope face and joint dip.  $F_3$  shows the connection between the slope face and the joint dips. In the case of planar slope failure,  $F_3$  is fair (-25) when the slope face and joint dips are parallel and unfavourable (-50) when the slope dips are 10° more than the joints (Singh and

Goel 1999).  $F_4$  pertains to the adjustment of the excavation method, and it refers to Romana (1985). A study using the RMR and SMR rock mass classifications to study slope stability in the Aceh Province was conducted by Rusydy et al. (2017, 2019). The RMR and SMR rock mass classifications are widely applied to study the probabilistic rock slope stability (Ersöz and Topal 2018).

## Results and discussions

### SRT and ERT survey

Two lines of SRT were measured both on the slope and on the side of the road to investigate sub-surface condition for the slope stability analysis. Figure 4 shows the measured

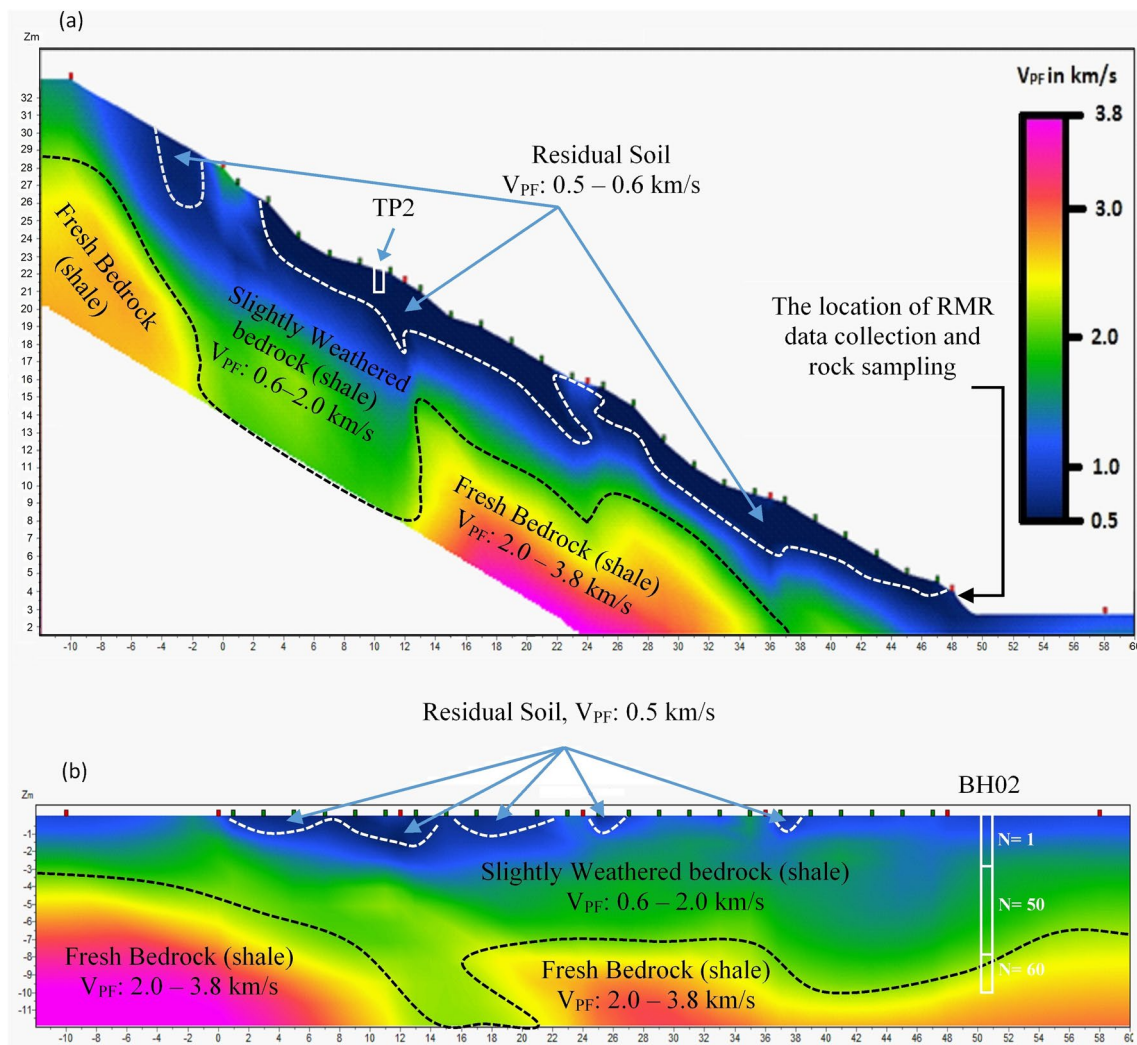


**Fig. 4** The SRT profile and the location of RMR data collection, i.e., at BH02 of TP2 site. The blue squares at the surface are the locations of the geophones measurements and the red squares are the locations

of shot points of the SRT source measurements **a** SRT profile on the slope, **b** SRT profile on the side of the road



points (in red squares) of the SRT profiles consisting of 7 shot points to ensure the sufficient and high-resolution results of  $V_{PF}$  to determine the slip zone for the landslide. Twenty four unit of geophones installed 2 m apart from one another. Herein, the geophone measured locations are indicated in blue squares appear on the surface in Fig. 4a, b. Overall, the total length of SRT longitudinal profile in this study makes up 68 m in total, and able to penetrate down to 12 m depth.

The SRT profile reveals several rock layers beneath the slope (see Fig. 4a) and the road (Fig. 4b). The P-wave velocities ( $V_{PF}$ ) obtained along the slope and the road is in the range of 0.5–3.8 km/s. These  $V_{PF}$  values divide sub-surface materials into three categories based on the result of the N-SPT measurement at BH02. The first material on the surface is loose soil ( $V_{PF}$  0.5–0.6 km/s) and it is part of the residual or depositional soil found on the surface of the slope; the layer thickness varies from 1 to 3 m on the slope. From this data, it can be interpreted that the possible slope failure for the residual soil on top of the rock layer is translation slope failure. On the road, the soft soil is only 1 m of thickness which has a  $V_{PF}$  of 0.5 km/s. The second layer beneath the soft soil had  $V_{PF}$  values ranging from 0.6 to 2 km/s interpreted to be slightly weathered shale which has several fractures both on the slope (see Fig. 4a) and on the road (see Fig. 4b). These weathered shale layers have  $V_{PF}$  values lower than the standard value of  $V_{PF}$  in shale and it similar to weathered shale studied by Lghoul et al. (2012). The first and second layers are separated by white dashed lines are interpreted as loose soil and slightly weathered shale; while the third layer on the slope is fresh shale and has  $V_{PF}$  values ranging from 2.0 to 3.6 km/s which are similar to fresh shale  $V_{PF}$  conducted by Awang et al. (2017) in Malaysia. In Fig. 4, the upper surface of the fresh shale is delineated by black dashed lines.

According to Cameron et al. (1982), shale in the investigated slope was originally formed in fluvial processes during the tertiary period. Due to chemical, mechanical, and biological weathering, this shale slowly decomposed to slightly, moderately, highly weathered shale, and residual soil by the end of the weathering process. All those degrees of weathering are revealed in SRT profile and these results are essential in developing slope material on slope stability simulation.

Two lines of ERT survey were conducted which location was immediately next to the seismic lines, both on the road slope and on the side of the road. ERT data processing are performed using Res2dinv software. It took eight iterations in the process resulting in a slope profile with RMR error 18.46%. On the side of the road, the ERT profile has a better result by went through merely two iterations, the RMR error merely 3.78%. For both profiles, the electrode spacings are 1.5 m which make up a total length of 81 m, with

corresponding penetration to approximately 17 m beneath the surface as shown in Fig. 5.

Figure 5 denotes the ERT profile on the slope and on the road where the value of soil resistivity is ranging from 9 to 53,000  $\Omega\text{m}$  (ohm-meter) on the slope (see Fig. 5a). The highest resistivity is found at a depth of 0 to 3 m, having resistivity value in the range of 150–54,000  $\Omega\text{m}$ ; as result, it is interpreted as soft or loose soil which has high porosity and is unsaturated to water. Below the soil layers, a low-resistivity stratum is found in the range of 9–150  $\Omega\text{m}$  at depth of 3–15 m, interpreted as shale layer with numerous fractures and saturated with groundwater. The groundwater layer in this shale rock is in a small amount because the shale is impermeable rock; as a consequence, the water only fills the fractures and the bedding aperture between shale layers. In Fig. 5a, the boundary between the shale and loose soil is illustrated as a black dashed line.

On the slope, the measurements were conducted in the same line for both seismic and ERT methods. Hence, they reveal similar patterns in sub-surface results. The boundary between loose soil and shale is demonstrated in the seismic and ERT data as the landslide slip zone. On the road, the resistivity values range from 52 to 483  $\Omega\text{m}$ ; fractures found in the road pavement allow water infiltration, which has a resistivity value from 52 to 100  $\Omega\text{m}$ . This groundwater is predicted based on the leakage of drainage system (see Fig. 5b), where the system next to the road is an earth-line drainage system; accordingly, the water from the road surface infiltrates to the sub-surface layer of the road, and further through the rock fractures.

The resistivity values from ERT profiles have successfully determined the water table (piezometric levels) on the slope and on the side of the road. The piezometric level due to the rainwater infiltration will induce resistivity variation of the soil beneath the slope, and it has been proved by Lebourg et al. (2010), Palis et al. (2017a), and Palis et al. (2017b). In addition, the resistivity values have been utilised by Uhlemann et al. (2017) to monitor the fluctuation of moisture contents on the slope, while Di Maio et al. (2020) determined the degree of saturation from resistivity values of the soil on the slope. Falae et al. (2019) emphasised the ERT method is capable to locate the high moisture content, the pathways of water drainages, and the groundwater circulation regime within an unstable area on the slope due to the resistivity contrast among geo-materials beneath the surface.

## Rock mass classification

Understanding the geological process and diagenesis of the rocks are a crucial part of studying rock slope stability. A sedimentary rock, such as shale, has a high degree of weathering especially when interacts with groundwater. The chemical weathering breaks down and changes shale

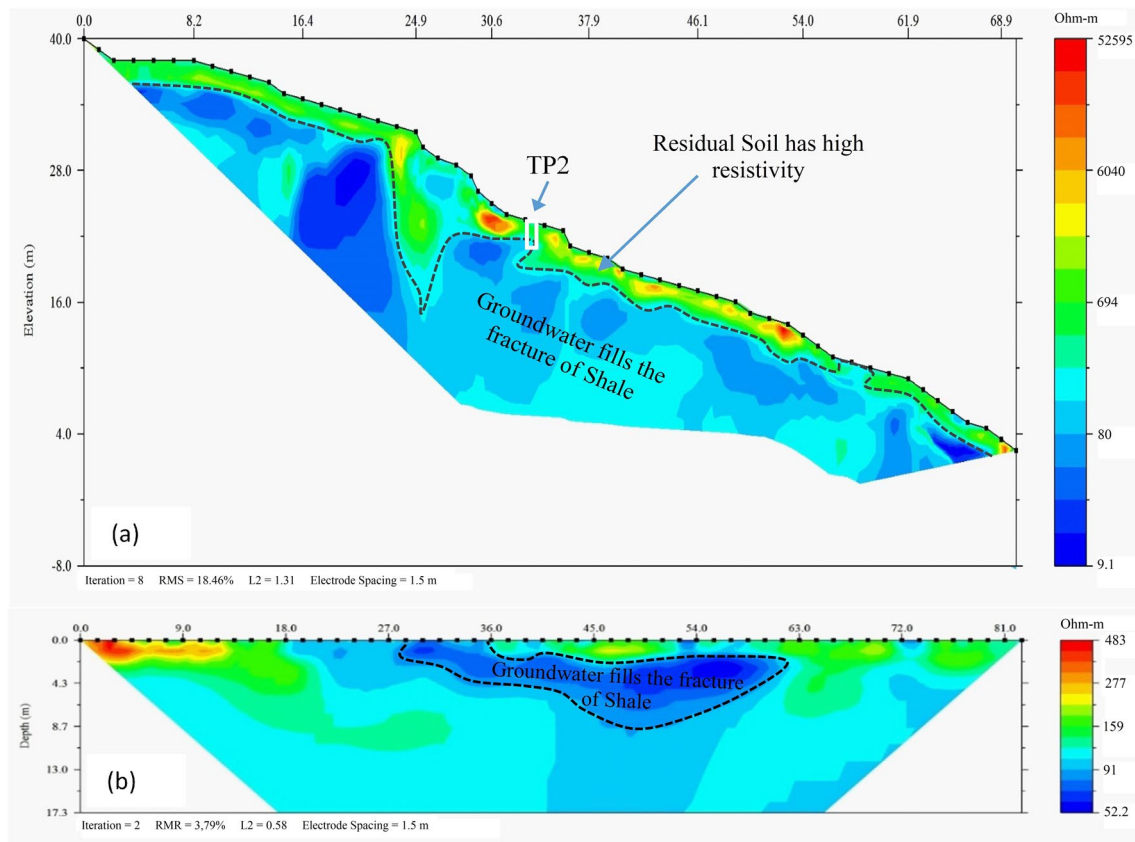


**Fig. 5** The ERT profile and its interpretation **a** On the slope and **b** On the side of the road

into a new substance, i.e., soil, by which more influential chemical weathering compares to the mechanical weathering. This fact will reduce rock mass quality over time; besides, tropical countries have very high rainfall intensity.

This study utilises the Bieniawski (1989)'s RMR parameters to calculate the total number of RMR as the number of rock mass quality, as shown in Table 1. The first parameter is the strength of intact rock revealed from a field measurement using the geological hammer. Herein, the results of UCS are in the range of 5–25 Mpa having two ratings. The RQD indicates the total distance higher than 10 cm dividing the total length of survey, the result reveals 85% of RQD. Most of the joints in the study area are formed as rock beddings with thickness are between 60 and 200 mm, and it is recognised as space of discontinuities. The joints condition of the rocks in the field are determined by their persistence, aperture, roughness, infilling materials, and weathering; which results of joint condition analyses can be seen in Table 2. As for the groundwater condition, the slope in Site A was wet, whilst in the site B was dripping. The result of the RMR values were 51 and 48, respectively (see Table 2), and according to Bieniawski (1989), both slopes will have an internal friction angle in the range of 25–35°. Furthermore, the structural geology

orientations were collected using the geological compass for both sites.

In site A, the geological survey recorded the slope orientation of 185° N for the slope face direction ( $\alpha_s$ ) and 30° for the slope dip angle ( $\beta_s$ ), while the bedding plane of the slope has a dip direction of 230°N ( $\alpha_j$ ) and a dip angle of 32° ( $\beta_j$ ). The slope strike and bedding strike are different by 45°; hence, according to slope kinematic analysis, there is no type of rock failure will occur at this specific study area (site A). In site B, the slope direction ( $\alpha_s$ ) is 220°N, and the slope angle ( $\beta_s$ ) is 30° while the dip direction ( $\alpha_j$ ) is 210°N, and the dip angle is 31° ( $\beta_j$ ). The planar rock slope failure is possible because of the parallelism between the slope and the rock joint by 10°, which is less than 20°, and the internal friction angle is lower than the dip angle. The types of failure in this analysis are utilized in calculating the SMR value (see Table 3).

### Geotechnical properties analysis

In BH01 and BH02, the  $N$ -value was found to be below 50 up to 3 m beneath the surface. Bowles (1979) noted that  $N > 50$  was classified as hard soil, which in this research was found at depths of 4 to 10 m. The soil description and

N-value for each depth are shown in Table 4. From the surface to 1 m for BH01 and up to 3 m for BH02, they have similar lithology consisting of clayey silt, coarse sand, and angular gravel, whereas the colour of the soil is brown; it has low water content and is slightly cohesive. At the depth of 1–4 m in BH01 and 3–8 m in BH02, this research found the fractured shale mixed with coarse sand, silt and less clay. The colour is brown with low water content and it is slightly

cohesive. This layer is defined as hard soil or a soft rock layer; BH01 only reached 4 m beneath the surface, but BH02 was up to 10 m thickness. From 8 to 10 m, we discovered a shale layer with a fair water content that is slightly cohesive; for detailed soil descriptions and the N-value for each layer, see Table 4. The disturbed soil sample was taken at a depth of 1 m in BH01 and 2.5 m in BH02. The soil property results are presented in Table 5.

**Table 2** The RMR results at site A and site B beneath the residual soil (the slightly weathered layer in Fig. 4a)

No	RMR Parameters	Site A		Site B	
		Condition	Rating	Condition	Rating
1	The strength of intact rock material	5–25 MPa	2	5–25 MPa	2
2	Rock Quality Designation (RQD)	85%	17	85%	17
3	Spacing of discontinuities	60–200 mm	8	60–200 mm	8
4	Condition of discontinuities				
	Persistence	10–20 m	1	10–20 m	1
	Aperture	< 0.1 mm	4	< 0.1 mm	4
	Roughness	Rough	5	Rough	5
	Infilling	Hard material < 5 mm	2	Hard material < 5 mm	2
	Weathering	Slightly weathered	5	Slightly weathered	5
5	Groundwater	Wet	7	Dripping	4
RMR		Fair Rock	51	Fair Rock	48
GSI		Fair	46	Fair	43

**Table 3** The SMR results at site A and site B beneath the residual soil

No.	SMR parameter	Site A		Site B	
		Condition for planar	Rating	Condition for planar	Rating
1	RMR	Fair Rock	51	Fair Rock	48
2	$F_1$	$(\alpha_s - \alpha_j) = 45^\circ$	0.09	$(\alpha_s - \alpha_j) = 10^\circ$	0.68
3	$F_2$	$\beta_j = 32^\circ$	0.62	$\beta_j = 31^\circ$	0.6
4	$F_3$	$\beta_j - \beta_s = 2^\circ$	- 6	$\beta_j - \beta_s = 1^\circ$	- 6
5	$F_4$	Natural slopes	15	Natural slopes	15
	SMR	Normal slope	65.66	Normal slope	60.55

**Table 4** Soil description details, the N-SPT value each layer for SPT data in BH01 and BH02, and the  $V_{PF}$  from SRT beside the road correlated with N-SPT value from BH02

BH 01			BH 02			
Depth (m)	Description of soil or rock material	N-SPT Value	Depth (m)	Description of soil or rock material	N-SPT Value	$V_{PF}$ (Km/s)
0–1	Claying silt, coarse sand, and angular gravel, brown colour, low moisture content, slightly cohesive	1	0–3	Claying silt, coarse sand, and angular gravel, brown colour, medium moisture content, slightly cohesive	1	0.6
1–4	Shale fragment with coarse sand, contains silt and a little clay, brown and blackish, low water content, solid, slightly cohesive	60	3–8	Shale mixed with silt and a little sand, brownish colour, medium moisture content, solid, slightly cohesive	50	2.0
			8–10	Dark gray colour shale, moderate water content, solid, slightly cohesive	60	2.5

**Table 5** The results of laboratory tests for the soil at BH01 and BH02

No.	Parameters	Notation	Unit	Disturbed sample	
				BH01	BH02
				Depth 1 m	Depth 2.5 m
1	Water content	$w$	%	8.361	19.089
2	Bulk density	$\gamma_b$	kN/m <sup>3</sup>	17.805	22.030
3	Dry density	$\gamma_d$	kN/m <sup>3</sup>	16.432	18.502
4	Specific gravity	$G_s$		2.723	2.767
5	Void ratio	$e$		0.630	0.470
6	Porosity	$n$		0.380	0.320
7	Degree of saturation	$S_R$	%	36.39	113.040
8	Liquid limit	LL	%	–	–
9	Plastic limit	PL	%	–	–
10	Plasticity index	PI	%	–	–
11	Sieve analysis				
	Gravel		%	7.870	51.800
	Sand		%	8.180	16.530
	Silt		%	57.520	12.570
	Clay		%	26.430	19.100

The types of soils on the slope are classified using AASHTO (America Association of State Highway and Transportation Officials) and USCS (The Unified Soil Classification System). The results of those classifications can be seen in Table 7; according to the USCS, the typology of soil on the slope is CL and ML-OL. Warren et al. (2016) noted that the ML type of soil under flowing groundwater conditions is assumed to exhibit zero to few rock-like properties; consequently, this group is defined as 0 RMR (Table 6).

**The empirical correlations**

**Geotechnical and geophysical correlations**

In this study, two SRT lines and two ERT lines were running over a road slope and over the side of a road where two N-SPT borehole and three pits tests were performed. The strength of correlations among the acquired data was subsequently analysed. From the seismic measurements, the  $V_{PF}$  values in Fig. 4b has a strong correlation with borehole data (BH02) situated on the side of the road (see Fig. 3). The correlation between  $V_{PF}$  values and N-SPT value from BH02 can be seen in Table 4. Several previous empirical studies have been conducted to reveal a linear correlation between  $V_{PF}$  value and N-SPT, such as

**Table 6** The results of laboratory tests for the soil on the slope and their physical characteristics to  $V_{PF}$  and Resistivity

No	Parameters	Notation	Unit	Undisturbed sample			$V_{PF}$ and resistivity	
				TP1	TP3	TP2	At 1.4 m (see Figs. 4a, 5a)	
				Depth 1.0 m	Depth 1.2 m	Depth 1.4 m	Previous study results	
1	Water content	$w$	%	30.971	23.272	15.943	320 $\Omega$ m	300 $\Omega$ m
2	Bulk density	$\gamma_b$	kN/m <sup>3</sup>	15.941	19.473	18.551	0.5 km/s	0.85 km/s
3	Dry density	$\gamma_d$	kN/m <sup>3</sup>	12.174	15.794	16.000	–	–
4	Specific gravity	$G_s$		2.739	2.795	2.748	–	–
5	Void ratio	$e$		1.210	0.740	0.680	–	–
6	Porosity	$n$		0.550	0.420	0.410	–	–
7	Degree of Saturation	$S_R$	%	70.230	88.400	63.960	–	–
8	Liquid limit	LL	%	30.324	29.520	36.176	–	–
9	Plastic limit	PL	%	21.800	23.220	29.530	–	–
10	Plasticity Index	PI	%	8.524	6.303	6.642	–	–
11	Sieve analysis							
	Gravel		%	16.880	7.830	14.070	–	–
	Sand		%	9.550	13.930	7.050	–	–
	Silt		%	15.480	51.580	46.180	–	–
	Clay		%	58.080	26.650	32.700	–	–
12	Direct shear							
	Cohesion	$c$	kN/m <sup>2</sup>	6.180	32.962	19.914	–	–
	Internal friction angle	$\phi$	(°)	16.330	24.040	24.320	–	–

Bery and Saad (2012), Awang and Mohamad (2016) indicating an increase in N-SPT value proportionately with the increase of  $V_{PF}$ , and went up with depth in sedimentary rock, which is similar to the result of this study (see Fig. 6). From the surface down to 3 m depth, the N-SPT value is 1, which is equivalent to 0.6 km/s of  $V_{PF}$ . At this certain depth, this study finds claying silt, coarse sand, angular gravel, and slightly cohesive, those characteristics interpreted as the topsoil. At a depth of 3 to 8 m, N-SPT value reveals 50 with  $V_{PF}$  is 2 km/s, which is recognised as slightly weathered bedrock mixing with silt and a little brownish sand. At a depth of 8 to 10 m, the N-SPT value reached 60 and it is equal to 2.5 km/s of  $V_{PF}$  where the dark grey fresh shale bedrock is found.

This study performed a regression analysis to produce an empirical correlation equation for  $N-SPT$  and  $V_{PF}$  denoted in Eq. 11. Illustrated in Fig. 6, the result of Eq. 11 stands in between Bery and Saad (2012), Awang and Mohamad (2016)'s trendlines. The  $t$ -test by employing the R Studio software reveals  $t$  value 10.211 and  $p$  value 0.06215, the correlation between  $N-SPT$  and  $V_{PF}$  is reliable, nevertheless it requires more data to approve this.

$$V_{PF} = 0.031(N - SPT) + 0.55 (R^2 = 0.99) \tag{11}$$

Furthermore, the undisturbed samples were taken from three test pits, TP1, TP2, and TP3; merely TP2 within 3 m from seismic and ERT survey lines on the slope. Hence, the geotechnical parameters obtained from TP2 are utilised in correlating with SRT characteristic  $V_{PF}$ , and the resistivity of soil which yield from ERT investigation and compare it with the previous study from Hua et al. (2020) and Fukue et al. (1999) as denoted in Table 6. From multitude geotechnical parameters yielded from the laboratory testing of TP2 sample, bulk density has a strong correlation with  $V_{PF}$  value from SRT and resistivity of soil with water content in the soil.

The  $V_{PF}$  value is escalating with the increase of material density, and the same pattern occurs for soil. From the undisturbed soil sample testing from TP2 at depth of 1.4 m, the bulk density of the soil is 18.551 kN/m<sup>3</sup>. At this certain depth, the  $V_{PF}$  value from SRT results in approximately 0.5 km/s as illustrated in Fig. 4a. Hua et al. (2020) developed the empirical relationship between soil bulk densities with  $V_{PF}$  value. Their empirical relationship shows that the soil bulk density 18.551 kN/m<sup>3</sup> will result the  $V_{PF}$  value about 0.85 km/s as denoted in Table 6. With merely 0.35 km/s

**Fig. 6** The correlation between investigated N-SPT and  $V_{PF}$  in this study compared to previous studies

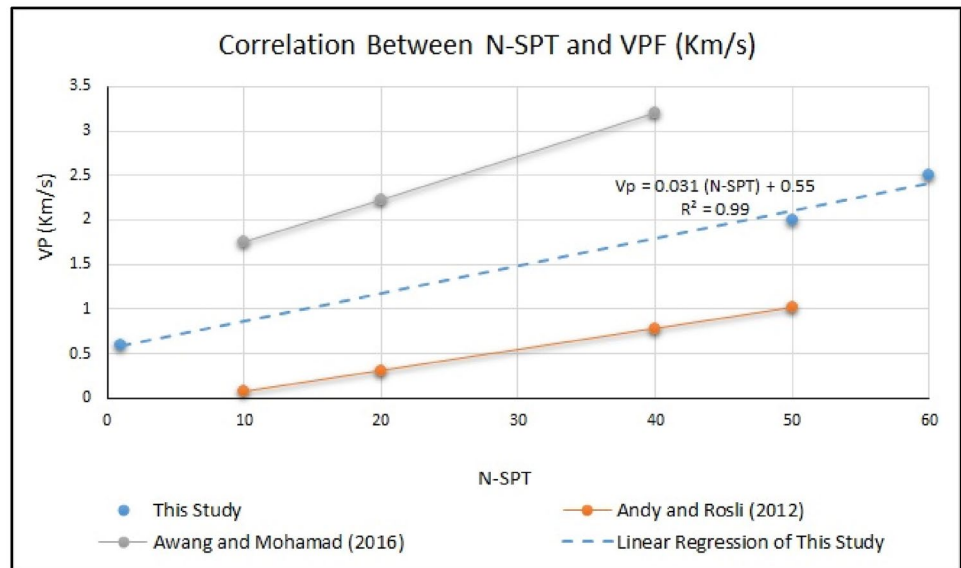


**Table 7** Soil Classification on the slope based on AASHTO and USCS

	USCS	Remarks	AASHTO	Soil Classifications
TP1	CL	Inorganic clays or low to medium plasticity, gravelly clays, sandy clays, lean clays	A-4	Silty soils
TP2	ML-OL	Inorganic silts and very fine sands, rock flour, silty or clayey fine sands with slight plasticity, or organic silt and organic silt-clay of low plasticity	A-4	Claying silt
TP3	ML-OL	Inorganic silts and very fines sands, rock flour, silty or clayey fine sands with slight plasticity. Or Organic silt and Organic silt-clay of low plasticity	A-4	Claying silt

difference, the results of both bulk density and  $V_{PF}$  value are reliable and can be utilised in the next analysis.

The resistivity of soil is declined with the increasing water content in the soil; thus, this study scrutinizes the resistivity value from the ERT profile shown in Fig. 5a overlapping with TP2. The resulting resistivity value is approximately  $320 \Omega\text{m}$  at the depth of 1.4 m, whilst the percentage of water content in TP2 at a similar depth is 15.943%. Also, a previous study by Fukue et al. (1999) on the correlation of soil water content with resistivity value was resulting in a 15.943% of soil water content yielded about  $300 \Omega\text{m}$  which is comparable with the resistivity value resulting from this study.

### Rock mass classifications and geophysical methods

The data acquisition for the RMR was conducted on the slope surface, as shown in Fig. 7a or in a slightly weathered layer where  $V_{PF}$  are 0.6–2.0 km/s. This layer has RMR value of 51 which is categorized as fair rock. Beneath this slightly weathered layer, as shown in Fig. 4a, fresh shale layers are found to produce high RMR values. Based on these surface RMR values, the GSI on sub-surface was calculated, as

shown in Table 2, and the SMR values are shown in Table 3. The SMR value of site A is different from that of site B due to different parallelism values in both slopes. Even though those slopes have different SMR values, according to RMR classification, both rock slopes are categorized as normal slopes and are partially stable.

The RMR, GSI, and SMR are the parameters in rock mass classifications for the rock surface, whilst the SRT result is utilized to determine the sub-surface value of RMR, GSI, and SMR. This study deploys Eqs. 5 and 7 to estimate the RMR and GSI values for the slightly weathered layer and fresh rock layer beneath the slope and Eq. 8, 9 and, 10 to compute the SMR. Equation 5 requires the  $V_{PF}$  value derived from SRT. Certainly, it can be used to estimate the RMR in assumptions that the rock mass beneath the slope is completely dry. Figure 7 shows the estimation result and the overlapping results between the SRT, the values of RMR, GSI, and SMR (Fig. 7a) and the ERT profile (Fig. 7b).

Table 2 indicates the real RMR, GSI, and SMR values derived from the geologic structure survey on the surface for Site A are 51, 46, and 65.6, respectively. Nevertheless, the calculated model (see Fig. 7a) yields a deviation. The values are varying from 53–56, 48–51, and 67–70 for RMR,

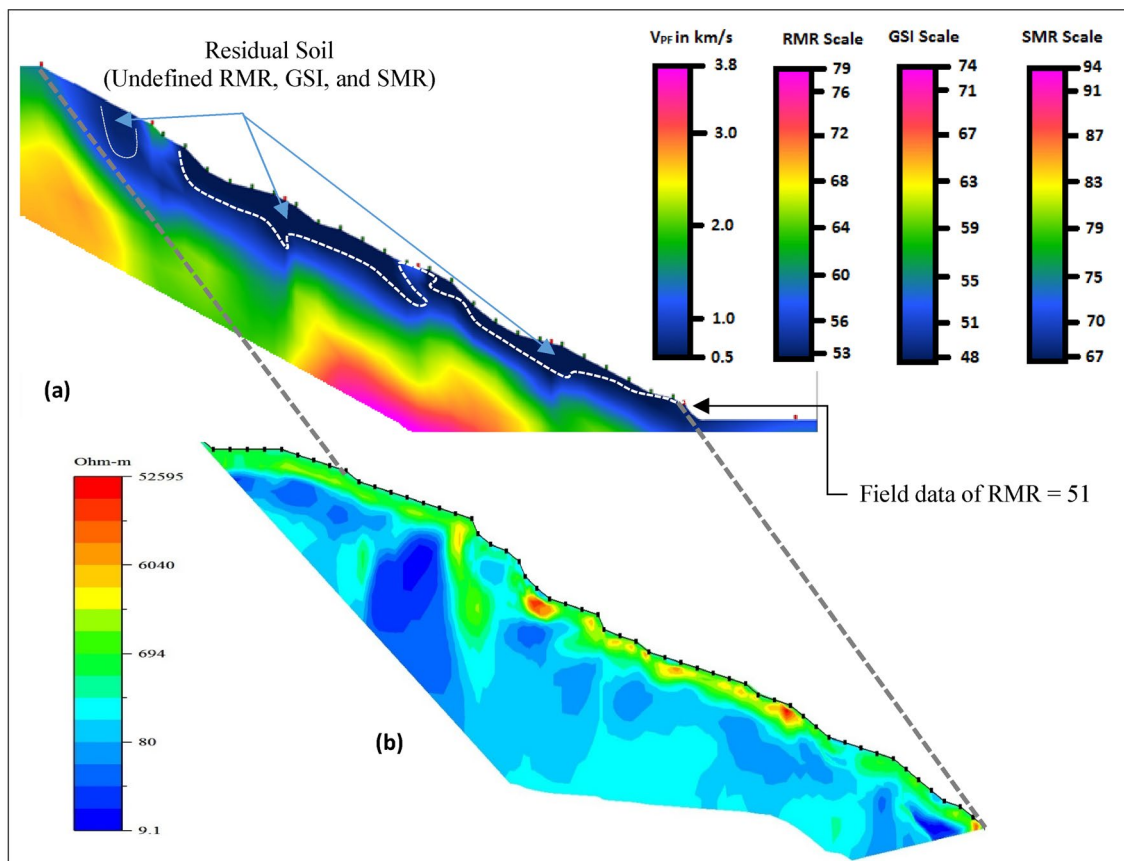


**Fig. 7** a The model of  $V_{PF}$  and calculated RMR, GSI, and SMR values, and b the ERT profile

GSI, and SMR, respectively. Equation 5 describes the relationships between RMR and  $V_{PF}$  proposed by Nourani et al. (2017). This equation initially has a regression of 0.794; moreover, when it is applied to this study area, the model RMR produced a higher value than the field data by 2–5 points. Since the deviation between the field data and the calculated ones is merely up to five points apart, it can be concluded that Eq. 5 is reliable in estimating the RMR value beneath the slope surface by applying the  $V_{PF}$ . For SMR calculation, the adjustment factors are assumed to be similar to both the surface as well as the sub-surface.

The values of RMR, GSI, and SMR have a different range in rock mass classifications. Bieniawski (1989) classified RMR values into five groups: very good (100–81), good (80–61), fair (60–41), poor (40–21), and very poor (<20). Hence, this research yields two classes of RMR beneath the slope; the fair rock class and the good rock class. The fair class in Fig. 7a is shown in blue, and good rock is in green to purple. The classification of the GSI system proposed by Hoek and Brown (1997) is similar to RMR; the rock classified as fair in GSI classification is shown in blue to green and good rock in yellow to purple. The estimation of SMR in the model is higher than the actual RMR and GSI.

### Slope stability simulation

In geotechnical engineering, apart from the rock condition, the stability of the slope is an important criterion for ensuring the connectivity of cities. Rock mass classification such as RMR and GSI help to compute the quality of the rock slope, whilst the SMR predicts the probability of rock slope failure but not being used to analyse the quality of the

soil-forming on top the rock. The rock mass classifications do not consider the force which acts in rock and soil-forming the slope; as a consequence, the numerical analysis is necessary to calculate the factor of safety. Furthermore, as a tropical and active tectonic country, the groundwater and the load from the earthquake affecting the stability of the slope must be considered and can only be solved by slope stability simulation.

The residual soil and the rock beneath were analysed and simulated by Slope/W software considering both the static groundwater and dynamic load from the earthquake. The geometry of the slope based on field measurement and the boundaries between soil and rocks beneath the surface derived from SRT and ERT models (see Figs. 4a and 5a). Those geophysical data are crucial for determining the sub-surface profile which is used in developing the slope stability simulation model. In static, this study considers the increasing groundwater. In the dynamic analysis, the only dynamic coefficient taken into account is the horizontal direction. The vertical direction is not taken into account since its effect to slope stability is not significant. Melo and Sharma (2004) suggested that the horizontal dynamic coefficient value used in the slope stability analysis is 40–45% of the peak ground acceleration (PGA). Considering the standard provided by the Ministry of Public Works and Housing (2011), the value of PGA for Aceh Province is 0.511 g; thus, the value of  $k_h$  used in the slope stability analysis in the dynamic condition is 0.204 g (40% from 0.511 g).

The input data of physical and mechanical parameters of the soil for the Slope/W software are based on the data from sample TP2 of site A and TP3 of site B as shown in Table 8, and Mohr–Coulomb model material is utilised for the soil on

**Table 8** Input Parameter to Slope/W software

Parameter	Model material	Site A	Site B
1. Residual soil	Mohr–Coulomb		
Saturated Density, $\gamma_{sat}$ (kN/m <sup>3</sup> )		19.990	19.950
Bulk Density, $\gamma_b$ (kN/m <sup>3</sup> )		18.550	19.470
cohesion, $c$ (kPa)		19.910	32.960
Internal friction angle, $\phi$ (degree)		24.320	24.040
2. Slightly weathered bedrock (shale)	Hoek–Brown failure criterion		
Bulk Density, $\gamma_b$ (kN/m <sup>3</sup> )		22.000	22.000
UCS of intact rock, $\sigma_{ci}$ (kPa)		5,000	5,000
$m_i$		4	4
GSI		46	43
$D$		0	0
3. Fresh bedrock (shale)	Hoek–Brown failure criterion		
Bulk Density, $\gamma_b$ (kN/m <sup>3</sup> )		24.00	24.00
UCS of intact rock, $\sigma_{ci}$ (kPa)		25,000	18,000
$m_i$		6	6
GSI		63	60
$D$		0	0

top of the rock, whereas the Hoek–Brown failure criterion is used for the rocks slope stability by applying Eq. 1 while additional parameters calculated using Eqs. 2, 3, and 4. The soil parameters were obtained from laboratory testing, the rock data were obtained from the field study, and the standard value was the one developed by Hoek et al. (2002).

In the static state, low groundwater level, the factor of safety for site A (see Fig. 8) and site B (see Fig. 9) are 1.058 and 1.182. At these factor of safety, the failure of the soil can occur in site A, while site B is safe. Yet, as the groundwater level escalates, the factor of safety for site A and B becomes 0.987 and 1.031, which are categorized as critical or unsafe. Being located in a tropical country, the rise of groundwater at the studied sites is highly likely to occur during the raining season, i.e., normally from September to February; thus, the slope stability changing conditions in a tropical country is seasonal. The laboratory tests reveal that the physical characteristics of the surface

soil is claying silt, coarse sand, angular gravel which have high hydrolic conductivity values or high permeability leading to high rate of rainwater infiltration to the slopes. In site B, the slope is stable during a dry season as the groundwater is lower. However, it is unstable during the rainy season. Overall, the worst-case scenario throughout the year considered as unstable.

As shown in Table 9, the slope simulation is modelled with two conditions, namely static and dynamic conditions. Each condition is modelled with two different groundwater levels to represent the ones during the dry season and rainy seasons. Based on the results of the simulation at the two observed sites, all conditions do not meet the slope stability criteria as the value of the safety factor in the static condition is less than 1.5 and in the dynamic condition is less than 1.0. In the static and dynamic condition with increasing groundwater level, the value of the safety factor is lower than that with low groundwater level. This explains that water can

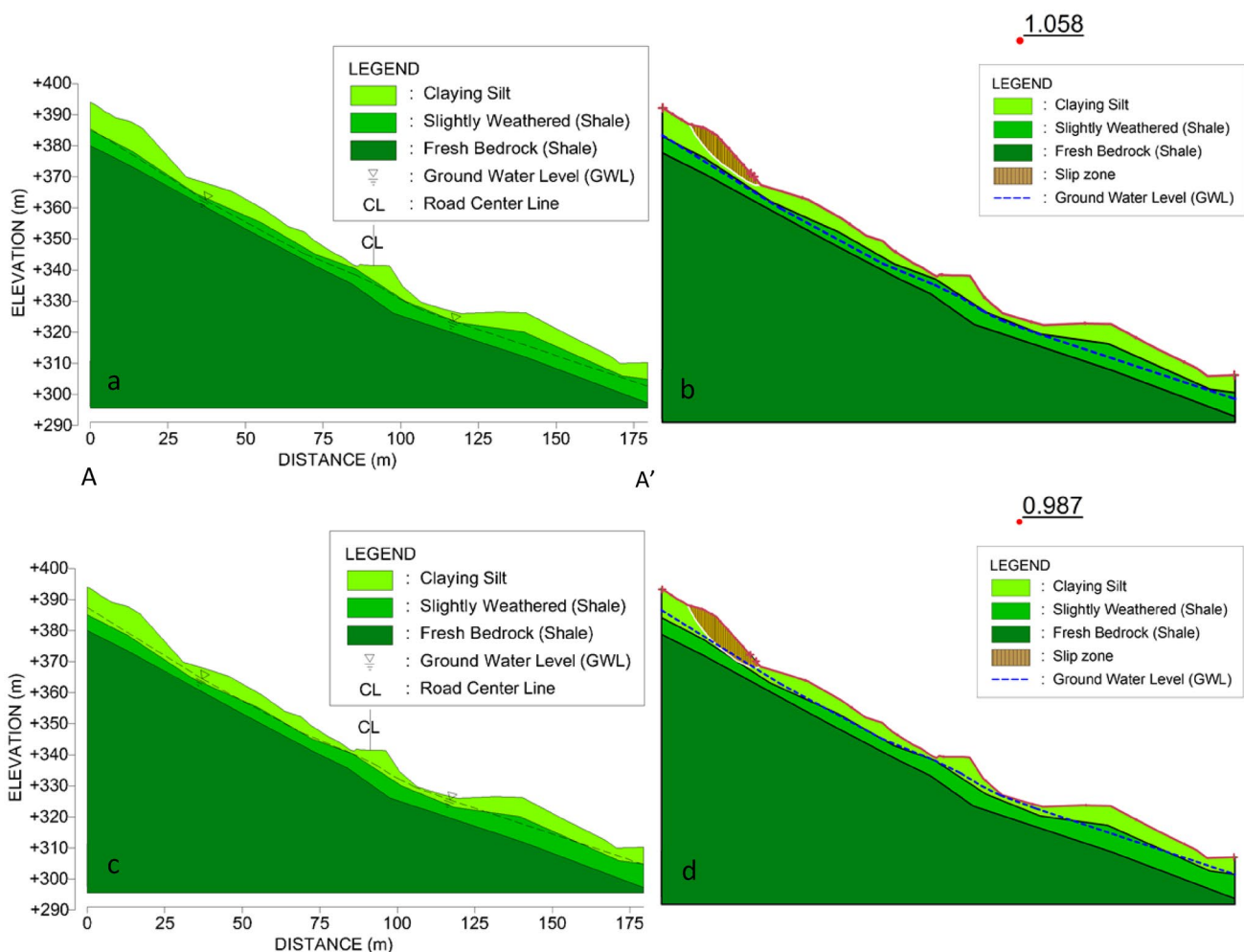


**Fig. 8** The static slope stability analyses for Site A, **a** cross section for lowers water table, **b** the result for lowers groundwater level, **c** cross section for increasing groundwater level, **d** the result of simulation for increasing water table



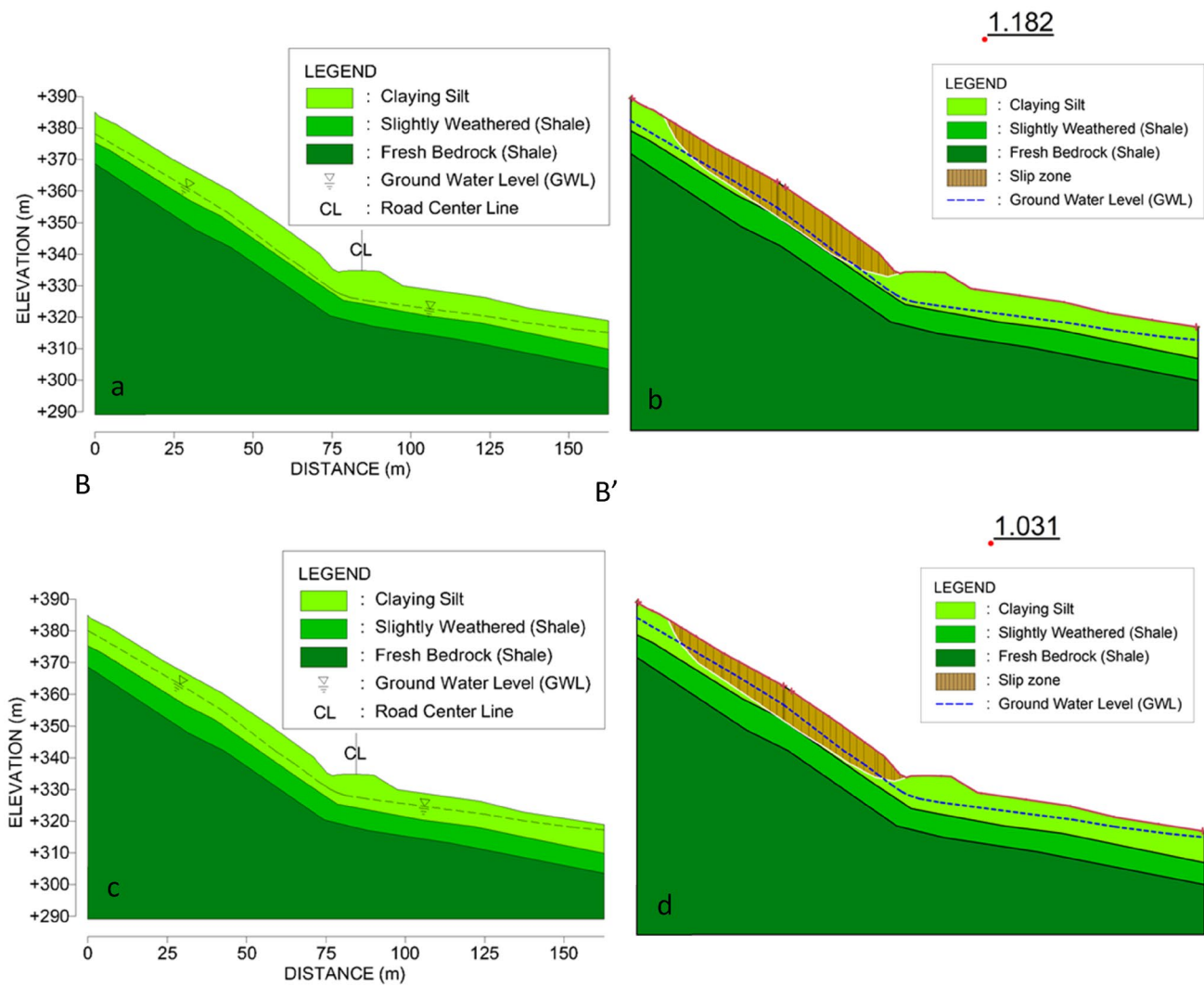


**Fig. 9** The static slope stability analyses for Site B, **a** cross section for lowers water table, **b** the result for lowers ground water level, **c** cross section for increasing groundwater level, **d** the result of simulation for increasing water table

**Table 9** The result of slope stability simulation at Site A and Site B

Location	Condition	Factor of Safety (FoS)	
		Static	Dynamic load (PGA = 0.204)
Site A	Low ground water level	1.058	0.784
	Increasing ground water level	0.987	0.756
Site B	Low ground water level	1.182	0.847
	Increasing ground water level	1.031	0.731

reduce the shear resistance in the slope; thus, reduce the slope stability.

In dynamic load due to earthquake, either in low ground-water level or in increasing groundwater level, both sites will have a critical condition or failure will occur. The detail

value descriptions for static and dynamic slope analysis at lower and higher groundwater are shown in Table 9. Besides, the ground shaking of the earthquake will reduce the stability of the slope either in the dry or rainy seasons. Therefore, slope stability in a tropical country which is prone to tectonic activities must consider the groundwater and dynamic load from earthquakes.

### Conclusion

The primary subjects govern the soil and rock slope stability are geology, hydrology, and seismology. All those subjects must be understood properly along with the methods in data acquisition from the field through the parameter inputs in slope stability simulation. All those subjects and methods

are presented and explain in this study as a contribution to the scientific community and practitioner working in slope stability research and projects. Regarding geology subject, this study reveals how the mechanical and physical properties of soil and rock are obtained from the field by combining the geophysical, engineering geology, and geotechnical approaches. As for hydrology, this study develops the slope stability considering the static stage of groundwater owing to dry and rainy sessions in a tropical country. The water table altitude relies on the result of the ERT survey. The dynamic effect from the earthquake is considered as the apart of seismology subject. The local tectonic which possibly trigger the earthquake must be scrutinised properly; therefore, the maximum peak ground acceleration (PGA) inputted to slope simulation process is reliable.

Slope stability in tropical and active tectonic countries must be analysed carefully and the integrated approaches including geophysics, engineering geology, and geotechnical methods are compulsory. Those approaches will yield more reliable results as conducted in this study which is successfully combined surface data from geotechnical methods and rock mass classification approaches along with sub-surface data collected by geophysical methods (SRT and ERT methods). Soil investigation in geotechnical approach found the linear correlation between the N-SPT values to  $V_{PF}$ . It indicates that the N-SPT investigation is probably to be replaced by the SRT survey to reduce the cost, increases efficiency, and to cover a large area in future. Previously, similar results related to empirical correlations between N-SPT to  $V_{PF}$  are conducted by Bery and Saad (2012), and Awang and Mohamad (2016); accordingly they revealed similar result to this study. Besides, the bulk density value also can be estimated from SRT and the water content from soil resistivity value in a ERT investigation. The slope stability simulation and analysis by considering the effect of groundwater and earthquakes using limit equilibrium analysis yield the reliable results and our study have successfully proved it. Hopefully, our approaches are considered as the role model for future research in studying soil and rock slope stability in tropical and active tectonic countries and it can be applied conveniently by other researchers. Furthermore, this study approach is recommended to be implemented in rock slope design to ensure the long-term safety of the road.

Even with the comprehensive approaches, this study still has limitations. This study only applied the deterministic method in computing the factor of safety (FoS) and the method does not consider the variability of physical and mechanical properties of soil and rock. Those properties are highly heterogeneous and can be solved by applying the probabilistic approach in slope stability simulation for future research. Besides, we suggest performing numerical modelling to examine the stresses and strains developed in the slope. Another suggestion is to conduct the rock degradation

analysis due to the chemical weathering; therefore, this phenomena must be scrutinised time-dependently, because the rate of weathering/degradation of rock in a tropical country is relatively very high. Accordingly, it will affect the quality of rock mass which is detrimental to rock slope stability in the long term.

**Acknowledgements** The authors would like to deliver our higher appreciation to Alex Kaminsky for allowing us to use the ZONDST2D software for SRT. We are also grateful to Mr. Syafrizal, Mr. Muzakir, and all of the students helping the authors during data acquisition and also to World Class Professor (WCP) Program of Kemenristekdikti 2018.

**Author contributions** IR, as data analysis on engineering geological data and manuscript preparation. TFF conducted rock and soil slope simulations and support on the interpretation of the results. NA and S, as geotechnical data analysis and interpretation. KI and EM as hydrologists for groundwater data analysis. KJ interpreted the seismic and geo-electrical data for slope stability.

**Funding** Publication of this paper was made based on WCP Program in Universitas Syiah Kuala, Ministry of Research, Technology, and Higher Education (RISTEKDIKTI) of Indonesia in 2018.

**Data availability** The datasets used and/or analyzed during the current study are available from the corresponding author on reasonable request.

## Compliance with ethical standards

**Conflict of interests** The authors declare that they have no competing interests.

## References

- Abdalla JA, Attom MF, Hawileh R (2015) Prediction of minimum factor of safety against slope failure in clayey soils using artificial neural network. *Environ Earth Sci* 73(9):5463–5477. <https://doi.org/10.1007/s12665-014-3800-x>
- Abramson LW, Lee TS, Sharma S, Boyce GM (2001) Slope stability and stabilization methods. John Wiley & Sons
- Andriani GF, Loiotine L (2020) Multidisciplinary approach for assessment of the factors affecting geohazard in karst valley: the case study of Gravina di Petruscio (Apulia, South Italy). *Environ Earth Sci* 79(19):1–16. <https://doi.org/10.1007/s12665-020-09212-y>
- ASTM D1586-11 (2011) Standard test method for standard penetration test (SPT) and split-barrel sampling of soils. ASTM International
- Avanzi GD, Galanti Y, Giannecchini R, Lo Presti D, Puccinelli A (2013) Estimation of soil properties of shallow landslide source areas by dynamic penetration tests: first outcomes from Northern Tuscany (Italy). *Bull Eng Geol Env* 72(3–4):609–624. <https://doi.org/10.1007/s10064-013-0535-y>
- Awang H, Mohamad MNN (2016) A correlation between P-wave velocities and standard penetration test (Spt-N) Blows Count for Meta-Sedimentary Soils of Tropical Country. In: *InCIEC 2015*. Springer, Singapore, pp 343–354. [https://doi.org/10.1007/978-981-10-0155-0\\_31](https://doi.org/10.1007/978-981-10-0155-0_31)
- Awang H, Rashidi NA, Yusof M, Mohammad K (2017) Correlation Between P-wave Velocity and Strength Index for Shale to Predict Uniaxial Compressive Strength Value. In: *MATEC*

- Web of Conferences 103. EDP Sciences, pp 07017. <https://doi.org/10.1051/mateconf/201710307017>
- Barber AJ, Crow MJ (2005) Pre-tertiary stratigraphy. In: Barber AJ, Crow MJ, Milson JS (eds) Sumatra: geology, resources, and tectonic evolution. Geological Society, London, p 41
- Barton NR, Lien R, Lunde J (1974) Engineering classification of rock masses for the design of tunnel support. *Rock Mech* 6(4):189–239. <https://doi.org/10.1007/BF01239496>
- Basahel H, Mitri H (2017) Application of rock mass classification systems to rock slope stability assessment: a case study. *J Rock Mech Geotech Eng* 9(6):993–1009. <https://doi.org/10.1016/j.jrmge.2017.07.007>
- Bery AA, Saad R (2012) Correlation of seismic P-wave velocities with engineering parameters (N value and rock quality) for tropical environmental study. *Int J Geosci* 3(4):749–757. <https://doi.org/10.4236/ijg.2012.34075>
- Bieniawski ZT (1989) Engineering rock mass classification. John Wiley & Sons, New York
- Bogoslovsky VA, Ogilvy AA (1997) Geophysical methods for the investigation of landslides. *Geophysics* 42(3):562–571. <https://doi.org/10.1190/1.1440727>
- Bowles JE (1979) Physical and geotechnical properties of soils. McGraw-Hill Book Company, New York
- Cameron NR, Bennet JD, Bridge DM, Djunuddin A, Ghazali SA, Harahap H, et al. (1982) Geologic map of Tapaktuan Quadrangle. North Sumatra, Bandung, Indonesia, Geological Research and Development Centre
- Das BM, Sobhan K (2013) Principles of geotechnical engineering. Cengage Learning, Boston (ISBN-10:1133108660)
- Di Maio R, De Paola C, Forte G, Piegari E, Pirone M, Santo A, Urcioli G (2020) An integrated geological, geotechnical and geophysical approach to identify predisposing factors for flowslide occurrence. *Eng Geol* 267:105473. <https://doi.org/10.1016/j.enggeo.2019.105473>
- Ersöz T, Topal T (2018) Assessment of rock slope stability with the effects of weathering and excavation by comparing deterministic methods and slope stability probability classification (SSPC). *Environ Earth Sci* 77(14):547. <https://doi.org/10.1007/s12665-018-7728-4>
- Falae PO, Kanungo D, Chauhan P, Dash RK (2019) Recent trends in application of electrical resistivity tomography for landslide study. In: Renewable energy and its innovative technologies. Springer, Berlin, 195–204
- Friedel S, Thielen A, Springman SM (2006) Investigation of a slope endangered by rainfall-induced landslides using 3D resistivity tomography and geotechnical testing. *J Appl Geophys* 60:100–114. <https://doi.org/10.1016/j.jappgeo.2006.01.001>
- Fukue M, Minato T, Horibe H, Taya N (1999) The micro-structures of clay given by resistivity measurements. *Eng Geol* 54(1–2):43–53. [https://doi.org/10.1016/s0013-7952\(99\)00060-5](https://doi.org/10.1016/s0013-7952(99)00060-5)
- Glade T, Stark P, Dikau R (2005) Determination of potential landslide shear plane depth using seismic refraction—a case study in Rheinhessen, Germany. *Bull Eng Geol Env* 64(2):151–158. <https://doi.org/10.1007/s10064-004-0258-1>
- Grelle G, Revellino P, Donnarumma A, Guadagno FM (2011) Bedding control on landslides: a methodological approach for computer-aided mapping analysis. *Nat Hazards Earth Syst Sci* 5(11):1395–1409. <https://doi.org/10.5194/nhess-11-1395-2011>
- Gunawan H, Al-Huda N, Sungkar M, Yulianur A, Setiawan B (2020) Slope stability analysis due to extreme precipitation. In: IOP Conference Series: Materials Science and Engineering 796 (1). IOP Publishing, pp 012044. <https://doi.org/10.1088/1757-899X/796/1/012044>
- Gurocak Z, Alemdag S, Zaman MM (2008) Rock slope stability and excavatability assessment of rocks at the Kapikaya dam site, Turkey. *Eng Geol* 96:17–27. <https://doi.org/10.1016/j.enggeo.2007.08.005>
- Hack R (2000) Geophysics for slope stability. *Surv Geophys* 21(4):423–448. <https://doi.org/10.1023/A:1006797126800>
- He H, Li S, Sun H, Yang T (2011) Environmental factors of road slope stability in mountain area using principal component analysis and hierarchy cluster. *Environ Earth Sci* 62(1):55–59. <https://doi.org/10.1007/s12665-010-0496-4>
- Hoek E (2007) Practical rock engineering, 1st edn. Canada, Rock Science. <https://www.rocksociety.com/documents/hoek/corner/Practical-Rock-Engineering-Full-Text.pdf>. Accessed 5 July 2016
- Hoek E, Brown ET (1997) Practical estimates of rock mass strength. *Int J Rock Mech Min Sci* 34(8):1165–1186. [https://doi.org/10.1016/S1365-1609\(97\)80069-X](https://doi.org/10.1016/S1365-1609(97)80069-X)
- Hoek E, Carranza-Torres C, Corkum B (2002) Hoek-Brown failure criterion-2002 edition. In: Proceedings of NARMS-Tac 1. Toronto, pp 267–273
- Hua T, Yang ZJ, Yang X, Huang H, Yao Q, Wu G, Li H (2020) Assessment of geomaterial compaction using the pressure-wave fundamental frequency. *Transport Geot* 22:100318. <https://doi.org/10.1016/j.trgeo.2020.100318>
- Isa SFM, Azhar ATS, Aziman M (2018) Design, operation and construction of a large rainfall simulator for the field study on Acidic Barren Slope. *Civil Eng J* 4(8):1851–1857. <https://doi.org/10.28991/cej-03091119>
- Jayawardena US, Izawa E (1994) A new chemical index of weathering for metamorphic silicate rocks in tropical regions: a study from Sri Lanka. *Eng Geol* 36(3–4):303–310. [https://doi.org/10.1016/0013-7952\(94\)90011-6](https://doi.org/10.1016/0013-7952(94)90011-6)
- Jongmans D, Garambois S (2007) Geophysical investigation of landslides: a review. *Bullet Soc Géol France* 178(2):101–112
- Kaminsky A (2015) ZondST2D—solution for near surface seismic. <https://www.linkedin.com/pulse/zondst2d-solution-near-surface-seismic-alex-kaminsky/>. Accessed 14 February 2018
- Kassou F, Bouziyane JB, Ghafiri A, Sabihi A (2020) Slope stability of embankments on soft soil improved with vertical drains. *Civil Eng J* 6(1):164–173. <https://doi.org/10.28991/cej-2020-03091461>
- Lebourg T, Hernandez M, Zerathe S, El Bedoui S, Jomard H, Fresia B (2010) Landslides triggered factors analysed by time lapse electrical survey and multidimensional statistical approach. *Eng Geol* 114(3–4):238–250. <https://doi.org/10.1016/j.enggeo.2010.05.001>
- Lghoul M, Teixidó T, Pena JA, Hakkou R, Kchikach A, Guérin R, Jaffal M, Zouhri L (2012) Electrical and seismic tomography used to image the structure of a tailings pond at the abandoned Kettara mine. *Morocco Mine Water Environ* 31(1):53–61. <https://doi.org/10.1007/s10230-012-0172-x>
- Liu Z, Wang H, Hantoro WS, Sathiamurthy E, Colin C, Zhao Y, Li J (2012) Climatic and tectonic controls on chemical weathering in tropical Southeast Asia (Malay Peninsula, Borneo, and Sumatra). *Chem Geol* 291:1–12. <https://doi.org/10.1016/j.chemgeo.2011.11.015>
- McCaffrey R (2009) The tectonic framework of the sumatran subduction zone. *Annu Rev Earth Planet Sci* 37:345–366. <https://doi.org/10.1146/annurev.earth.031208.100212>
- Melo C, Sharma S (2004) Seismic coefficients for pseudostatic slope analysis. In: 13 th World Conference on Earthquake Engineering. Vancouver, Canada, Paper No. 369
- Ministry of Public Works and Housing (2011) Spectra Design of Indonesia. Centre of Research and Development—Ministry of Public Works and Housing of Indonesia. [http://puskim.pu.go.id/Aplikasi/desain\\_spektra\\_indonesia\\_2011/](http://puskim.pu.go.id/Aplikasi/desain_spektra_indonesia_2011/). Accessed 14 November 2018
- Mohammadi M, Hossaini MF (2017) Modification of rock mass rating system: Interbedding of strong and weak rock layers. *J Rock Mech Geotech Eng* 9(6):1165–1170. <https://doi.org/10.1016/j.jrmge.2017.06.002>

- Muksin U, Rusydy I, Erbas K, Ismail N (2018) Investigation of aceh segment and seulimeum fault by using seismological data; a preliminary result. In: *Journal of Physics: Conference Series*. 1011. IOP Publishing, pp 012031. <https://doi.org/10.1088/1742-6596/1011/1/012031>
- Nourani MH, Moghadder MT, Safari M (2017) Classification and assessment of rock mass parameters in Choghart iron mine using P-wave velocity. *J Rock Mech Geotech Eng* 9(2):318–328. <https://doi.org/10.1016/j.jrmge.2016.11.006>
- Palis E, Lebourg T, Tric E, Malet JP, Vidal M (2017a) Long-term monitoring of a large deep-seated landslide (La Clapiere, South-east French Alps): initial study. *Landslides* 14(1):155–170. <https://doi.org/10.1007/s10346-016-0705-7>
- Palis E, Lebourg T, Vidal M, Levy C, Tric E, Hernandez M (2017b) Multiyear time-lapse ERT to study short- and long-term landslide hydrological dynamics. *Landslides* 14(4):1333–1343. <https://doi.org/10.1007/s10346-016-0791-6>
- Palmstrom A (2005) Measurements of and correlations between block size and rock quality designation (RQD). *Tunnels Underground Space Tech* 20:362–377. <https://doi.org/10.1016/j.tust.2005.01.005>
- Rai MA, Kramadibrata S, Wattimena RK (2014) *Mekanika Batuan*. Penerbit ITB, Bandung (in Indonesian language)
- Romana M (1985) New adjustment ratings for application of Bieniawski classification to slopes. In: *proceedings of international symposium on the role of rock mechanics*. Zacatecas, ISRM, pp 49–53
- Rusydy I, Sugiyanto D, Satrio L, Rahman A, Munandar I (2016) Geological aspect of slope failure and mitigation approach in bireuntakengon main road, Aceh Province, Indonesia. *Aceh Int J Sci Technol* 5(1):30–37. <https://doi.org/10.13170/aijst.5.1.3841>
- Rusydy I, Al-Huda N, Jamaluddin K, Sundary D, Nugraha GS (2017) Analisis Kestabilan Lereng Batu Di Jalan Raya Lhoknga Km 17, 8 Kabupaten Aceh Besar. *RISSET Geol Pertambangan* 27(2):145–155. <https://doi.org/10.14203/risetgeotam2017.v27.452> (in Indonesian language)
- Rusydy I, Muksin U, Mulkal, Idris Y, Akram MN, Syamsidik (2018) The prediction of building damages and casualties in the Kuta Alam sub district-Banda Aceh caused by different earthquake models. In: *AIP Conference Proceedings* 1987(1). AIP Publishing LLC, pp 020012. <https://doi.org/10.1063/1.5047297>
- Rusydy I, Al-Huda N, Fahmi M, Effendi N (2019) Kinematic analysis and rock mass classifications for rock slope failure at USAID highways. *Struct Durability Health Monitoring* 13(4):379–398. <https://doi.org/10.32604/sdhm.2019.08192>
- Rusydy I, Idris Y, Muksin U, Cummins P, Syamsidik AMN (2020a) Shallow crustal earthquake models, damage, and loss predictions in Banda Aceh, Indonesia. *Geoenviro Disasters* 7(1):8. <https://doi.org/10.1186/s40677-020-0145-5>
- Rusydy I, Setiawan B, Zainal M, Idris S, Basyar K, Putra YA (2020b) Integration of borehole and vertical electrical sounding data to characterise the sedimentation process and groundwater in Krueng Aceh basin, Indonesia. *Groundwater Sustain Dev* 10:100372. <https://doi.org/10.1016/j.gsd.2020.100372>
- Rusydy I, Al-Huda N, Fahmi M, Effendi N, Muslim A, Lubis M (2020c) Analisis modulus deformasi massa batuan pada segmen jalan USAID Km 27 Hingga Km 30 Berdasarkan Klasifikasi Massa Batuan. *RISSET Geol Pertambangan* 30(1):93–105. <https://doi.org/10.14203/risetgeotam2020.v30.1073>
- Siddique T, Khan EA (2019) Stability appraisal of road cut slopes along a strategic transportation route in the Himalayas, Uttarakhand. *India SN Appl Sci* 1(5):409. <https://doi.org/10.1007/s42452-019-0433-4>
- Singh B, Goel RK (1999) *Rock mass classification. A practical approach in civil engineering*. Elsevier, Amsterdam
- Sugiyanto D, Rusydy I, Marwan M, Hidayati DM, Asrillah A (2018) A Preliminary study on aquifer identification based on geo-electrical data in Banda Aceh Indonesia. *J Natural* 18(3):122–126. <https://doi.org/10.24815/jn.v18i3.11204>
- Syukri M, Taib AM, Fadhli Z, Safitri R (2020) Geophysical investigation of road failure the case of the main street of Alue Naga, Banda Aceh, Indonesia. In: *IOP Conference Series: Materials Science and Engineering* 933(1). IOP Publishing, pp 012056. <https://doi.org/10.1088/1757-899X/933/1/012056>
- Telford WM, Geldart LP, Sheriff RE (1990) *Applied geophysics*, 2nd edn. Cambridge University Press, Cambridge
- Uhlemann S, Chambers J, Wilkinson P, Maurer H, Merritt A, Meldrum P, Kuras O, Gunn D, Smith A, Dijkstra T (2017) Four-dimensional imaging of moisture dynamics during landslide reactivation. *J Geophys Res: Earth Surface* 122(1):398–418. <https://doi.org/10.1002/2016JF003983>
- Wang B, Huang F, Wu Z, Yang J, Fu X, Kikuchi K (2009) Multi-scale climate variability of the South China Sea monsoon: a review. *Dyn Atmos Oceans* 47(1–3):15–37. <https://doi.org/10.1016/j.dynatmoce.2008.09.004>
- Warren SN, Kallu RR, Barnard CK (2016) Correlation of the Rock Mass Rating (RMR) System with the Unified Soil Classification System (USCS): introduction of the weak rock mass rating system (W-RMR). *Rock Mech Rock Eng* 49:4507–4518. <https://doi.org/10.1007/s00603-016-1090-1>
- Wei Y, Jiabin L, Zonghong L, Wei W, Xiaoyun S (2020) A strength reduction method based on the Generalized Hoek-Brown (GHB) criterion for rock slope stability analysis. *Comput Geotech* 117:103240. <https://doi.org/10.1016/j.compgeo.2019.103240>
- Wyllie DC, Mah C (2004) *Rock slope engineering*, 4th edn. Spoon Press, London
- Xue D, Li T, Zhang S, Ma C, Gao M, Liu J (2018) Failure mechanism and stabilization of a basalt rock slide with weak layers. *Eng Geol* 233:213–224. <https://doi.org/10.1016/j.enggeo.2017.12.005>
- Zikrilah M, Sugiyanto D, Rusydy I (2016) Identification of sub-surface structure using seismic refraction method At Jantho Aceh Besar. *J Natural* 16(2):1–4

**Publisher's Note** Springer Nature remains neutral with regard to jurisdictional claims in published maps and institutional affiliations.